

The Impact of γ Radiation on the Bioavailability of Fe(III) Minerals for Microbial Respiration

Ashley R. Brown,^{*,†,‡} Paul L. Wincott,^{†,∇} Jay A. LaVerne,[§] Joe S. Small,^{||} David J. Vaughan,[†] Simon M. Pimblott,^{‡,⊥,#} and Jonathan R. Lloyd^{†,‡}

[†]School of Earth, Atmospheric and Environmental Sciences and Williamson Research Centre for Molecular Environmental Science, The University of Manchester, Manchester, M13 9PL, U.K.

[‡]Research Centre for Radwaste and Decommissioning, The University of Manchester, Manchester, M13 9PL, U.K.

[§]Department of Physics and Radiation Laboratory, University of Notre Dame, Notre Dame, Indiana 46556, United States

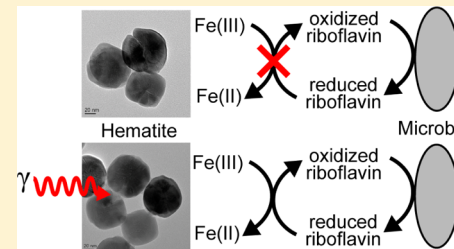
^{||}National Nuclear Laboratory, Birchwood Park, Warrington, WA3 6AE, U.K.

[⊥]School of Chemistry and Dalton Nuclear Institute, The University of Manchester, Manchester, M13 9PL, U.K.

[#]Dalton Cumbrian Facility, Westlakes Science & Technology Park, Moor Row, CA24 3HA, U.K.

Supporting Information

ABSTRACT: Conservation of energy by Fe(III)-reducing species such as *Shewanella oneidensis* could potentially control the redox potential of environments relevant to the geological disposal of radioactive waste and radionuclide contaminated land. Such environments will be exposed to ionizing radiation so characterization of radiation alteration to the mineralogy and the resultant impact upon microbial respiration of iron is essential. Radiation induced changes to the iron mineralogy may impact upon microbial respiration and, subsequently, influence the oxidation state of redox-sensitive radionuclides. In the present work, Mössbauer spectroscopy and electron microscopy indicate that irradiation (1 MGy gamma) of 2-line ferrihydrite can lead to conversion to a more crystalline phase, one similar to akaganeite. The room temperature Mössbauer spectrum of irradiated hematite shows the emergence of a paramagnetic Fe(III) phase. Spectrophotometric determination of Fe(II) reveals a radiation-induced increase in the rate and extent of ferrihydrite and hematite reduction by *S. oneidensis* in the presence of an electron shuttle (riboflavin). Characterization of bioreduced solids via XRD indicate that this additional Fe(II) is incorporated into siderite and ferrous hydroxy carbonate, along with magnetite, in ferrihydrite systems, and siderite in hematite systems. This study suggests that mineralogical changes to ferrihydrite and hematite induced by radiation may lead to an increase in bioavailability of Fe(III) for respiration by Fe(III)-reducing bacteria.



INTRODUCTION

Fe(III)-reducing bacteria such as *Shewanella oneidensis* couple the oxidation of organic matter to the reduction of a range of redox active metals and radionuclides. This may occur directly, via enzymatic reduction of redox active metal contaminants and radionuclides, or indirectly, via the reduction of bioavailable Fe(III) and subsequent abiotic electron transfer from Fe(II) to other metals and radionuclides.^{1–4} Hence, the biogeochemical cycling of iron can impart a control on the redox potential of environments relevant to the geological disposal of radioactive waste and radionuclide contaminated land. For instance, the precipitation of some redox sensitive radionuclides such as Tc(VII) and U(VI) can be achieved by their reduction to insoluble Tc(IV) and U(IV) species.^{5,6} Similarly, toxic and mobile contaminants such as chromium can also be removed from solution by the reduction of Cr(VI) to the less toxic Cr(III).^{3,7} Thus, dissimilatory iron-reducing species such as *Shewanella* sp. and *Geobacter* sp. have been considered for the remediation of complex wastes, including contaminant metals

and radionuclides and also toxic organic compounds that can be degraded by these organisms.⁸

Remediation of such environments presents a challenge as sites contaminated with radionuclides may exhibit large fluxes of ionizing radiation.⁷ Similarly, the geological disposal of intermediate and high level nuclear wastes (ILW/HLW) involves the packaging of highly radioactive wastes (activities exceeding 4 GBq metric ton⁻¹ alpha or 12 GBq metric ton⁻¹ beta/gamma), which may require shielding to reduce dose during transport and operations.⁹ Dose rates are expected to be variable due to the dynamics of radioactive decay of a range of fission and activation products and longer-lived actinides; however, absorbed doses over the life of a repository may be significant.¹⁰

Received: February 11, 2014

Revised: August 27, 2014

Accepted: August 28, 2014

Published: September 8, 2014



Container materials for the packaging of intermediate level waste include iron rich materials, such as stainless and carbon steel, which will likely receive significant doses of ionizing radiation. Subsequent interactions between radiolysis products and steel may generate a range of iron oxides, including maghemite ($\gamma\text{-Fe}_2\text{O}_3$), goethite ($\alpha\text{-FeOOH}$), and lepidocrocite ($\gamma\text{-FeOOH}$).^{11,12} In addition, some waste forms may contain large quantities of steels and their corrosion products and may also include Fe hydroxide floc from effluent treatment.⁹ These components would also be subject to a radiation flux.

Due to the redox sensitivity of iron, it is possible to observe a range of radiation-induced oxidation and reduction reactions depending on the initial oxidation state and coordination chemistry of the iron. For example, Ladrière¹³ notes that both oxidation and reduction of the iron is visible in the Mössbauer spectra of gamma irradiated iron-containing compounds. In this case, the formation of radicals in the first coordination sphere of the iron induces any reduction/oxidation. In aqueous systems, however, oxidizing and reducing species generated by the gamma radiolysis of water, such as $\cdot\text{OH}$, e^-aq , H^\bullet , HO_2^\bullet , H_2 , H_2O_2 , H^+aq are likely to dominate the redox potentials at the surface of iron-bearing compounds and, hence, facilitate their corrosion.^{11,12}

The oxidation state of iron in part governs crystal structure, surface area and reactivity¹⁴ and these parameters act as constraints on the thermodynamics of microbial iron reduction.^{15–18} Consequently, the radiation driven alteration of iron oxides, including any potential changes in crystal structure and oxidation state may impact upon microbial respiration of Fe(III)-bearing phases. Perturbations to the biogeochemical cycling of this iron may subsequently affect the solubility and mobility of radionuclides. Hence, characterization of radiation alteration of a range of environmentally relevant iron oxides, and the resultant impact upon microbial respiration of iron, may be important in understanding the behavior of redox-sensitive radionuclides and their treatment in safety cases, which must be constructed as part of the regulatory process underpinning geological disposal facilities for radioactive waste.

In this study, suspensions of ferrihydrite and hematite were irradiated with 1 MGy of γ radiation in order to assess the impact of radiation on these minerals and to identify subsequent changes in the availability of Fe(III) for microbial respiration. Previous workers have suggested gamma and neutron absorbed doses near high-level waste container surfaces may be in the region of 0.7 MGy after 10^4 years.^{19,20} For clays, which may be used as backfill material, total absorbed doses in the order of MGy to GGy have also been suggested.²¹ While it is difficult to predict total absorbed doses for iron mineral phases in the near field of a geological disposal facility, 1 MGy gamma was chosen to allow a phenomenological investigation rather than to accurately simulate conditions expected in a geological disposal facility.

Here we report on the radiation induced alteration of hematite and ferrihydrite as characterized using transmission electron microscopy (TEM), including selected area electron diffraction (SAED), and Mössbauer spectroscopy. Ferrozine assay was used to evaluate the postirradiation availability of these Fe(III) minerals for reduction by *S. oneidensis*, a model dissimilatory Fe(III)-reducing bacterium. This study is the first in which an attempt is made to document enhanced microbial Fe(III)-reduction as a result of radiation driven alterations to iron oxides.

EXPERIMENTAL SECTION

Mineral Synthesis and Irradiation. Hematite and 2-line ferrihydrite were synthesized by methods described in the Supporting Information (SI) section. The structures of the synthesized minerals were confirmed by X-ray (powder) diffraction (XRD) using a *Bruker D8 Advance* instrument with Cu $K_{\alpha 1}$ radiation. Samples consisting of a suspension of the mineral with 1 mL of 480 mM Fe were then placed into ampules and flame-sealed, autoclaved and treated, as appropriate, with 1 MGy γ radiation in a Shepherd ^{60}Co source. The dose rate was approximately 200 Gy min⁻¹, as determined by the Fricke dosimeter.

Mineralogical Characterization. Postirradiation samples of hematite and ferrihydrite were characterized using transmission electron microscopy (TEM) also involving selected area electron diffraction (SAED). Samples were prepared by suspending in ethanol prior to drop-casting onto carbon support films (Agar Scientific). Bright field TEM images were acquired using a Philips microscope fitted with a 200 keV field emission gun and gatan imaging filter (GIF200). SAED patterns for all samples were acquired using an appropriate aperture and *d*-spacings were measured and compared to reference iron oxides.²²

For Mössbauer spectroscopy, irradiated minerals were dried inside a desiccator within an anoxic cabinet. Where a volume of powder was insufficient for short analysis times, powders were mixed with boron nitride. Dried powders were then sealed anaerobically inside polyethylene mounts using epoxy sealant. Mössbauer spectra were collected at room temperature using a ^{57}Co source. Iron was used for calibration and all isomer shifts are reported with metallic $\alpha\text{-Fe}$ foil as the reference material. Data were acquired and processed using the *Recoil* Program (University of Ottawa). Lorentzian fits were used to model the spectra. For all fits, unless otherwise noted, the isomer shift, quadrupole splitting, hyperfine parameter, half width at half-maximum and relative areas of peaks were allowed to float during fitting.

Microbial Fe(III) Reduction. *S. oneidensis* MR-1 was grown aerobically in tryptic soy broth in Erlenmeyer flasks at 30 °C and shaken at 130 rpm. This starting culture was then used to inoculate a fully defined, sterile, nitrogen sparged minimal medium based on that of Myers and Nealson,²³ using 100 mM lactate and 20 mM fumarate as the electron donor and acceptor respectively (see SI for full recipe). After 24 h incubation at 30 °C, late log-early stationary phase biomass was harvested by centrifugation at 4920g for 20 min at 4 °C and, then, washed twice in sterile 30 mM sodium bicarbonate buffer in an 80:20 gas mix of N₂:CO₂. Aliquots of the buffered cell suspension (0.2 mL) were added to 9 mL anaerobic 30 mM bicarbonate buffer containing 50 mM lactate as electron donor. The final cell optical density of 0.4, measured at 600 nm using a UV-vis spectrophotometer, was equivalent to approximately 7×10^8 cells mL⁻¹. One mL aliquots of Fe mineral suspension were added to produce a final Fe concentration of 10 mM. Riboflavin (10 μM) was added as an electron shuttle as necessary. Triplicate experiments, along with sterile controls, were incubated in the dark at 30 °C.

Each experimental bottle was shaken and then sampled periodically (anaerobically and aseptically) for 0.5 N HCl extractable Fe(II) with Fe concentrations determined by ferrozine assay with the absorbance at 562.0 nm measured using a UV-vis spectrophotometer (Jenway).^{24,25} 24 h 0.5 and

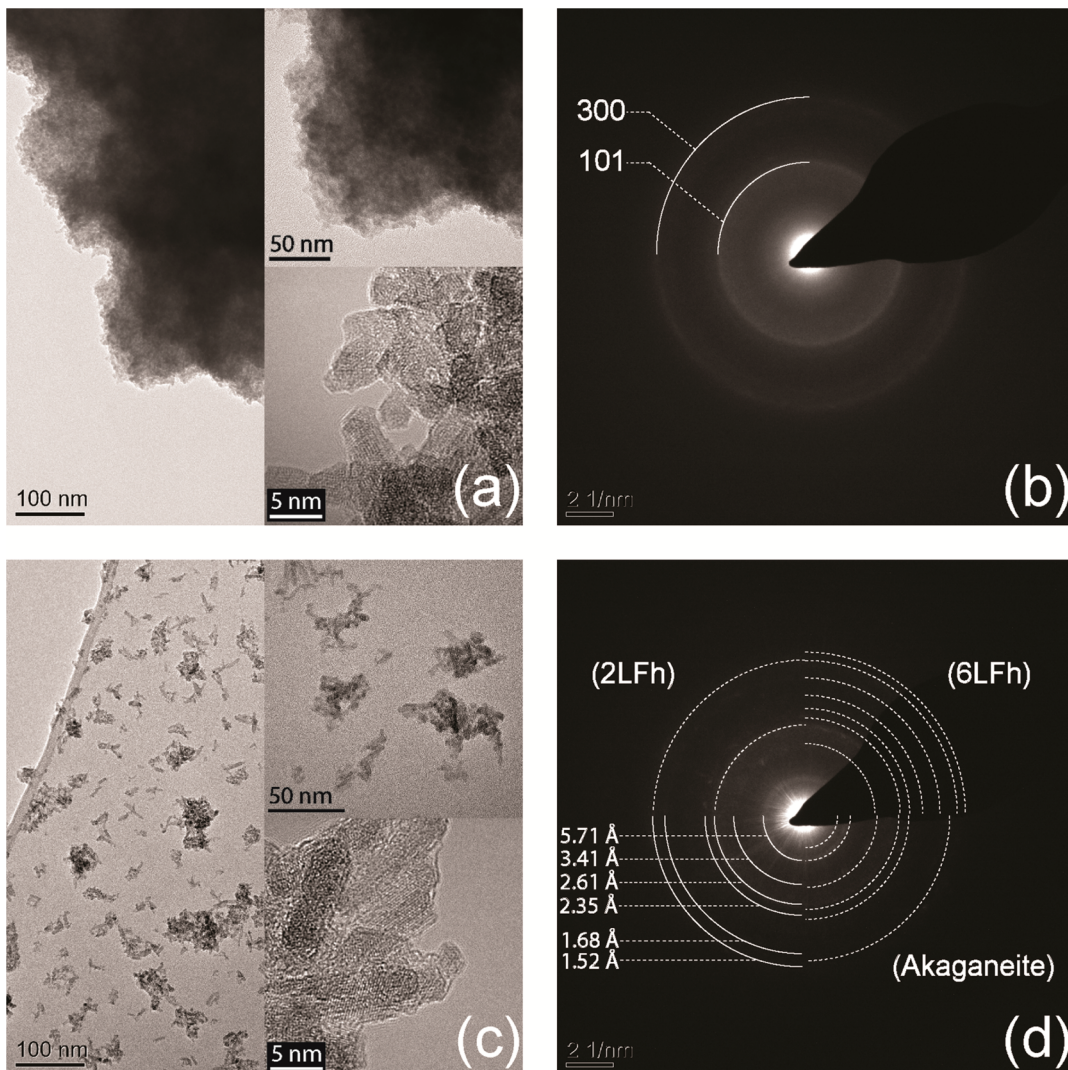


Figure 1. Transmission electron micrographs of (a) nonirradiated ferrihydrite and (c) irradiated ferrihydrite. The corresponding SAED pattern for nonirradiated ferrihydrite is shown in (b) with indexed lines for 2-line ferrihydrite. The corresponding SAED pattern for irradiated ferrihydrite is shown in (d) with measured interplanar spacings for irradiated suspensions in the bottom left segment and remaining segments displaying previously reported indexed patterns for selected Fe(III)-(oxy)hydroxides.

3 N HCl digests with the addition of 0.25 N hydroxylamine-HCl were utilized to determine total Fe concentrations in ferrihydrite and hematite experiments, respectively.

At the end of each experiment, the solid material was removed from suspension by centrifugation at 5000g for 20 min under anoxic conditions. The solids were then washed twice using 5 mL anaerobic deionized H₂O and centrifuged and resuspended between each washing step. The material was dried under N₂ (2% H₂). The bioreduced solids were then characterized using powder XRD and Mössbauer spectroscopy as described earlier.

RESULTS AND DISCUSSION

Mineralogical Characterization of Irradiated Fe(III) Oxides. To identify any structural changes that could influence the bioavailability of the irradiated Fe(III) phases, samples were examined using TEM. The TEM images of nonirradiated ferrihydrite displayed a morphology typical of amorphous 2-line ferrihydrite (Figure 1a)²⁶ and SAED patterns contained reflections attributable to 2-line ferrihydrite (Figure 1b).^{27–29}

Irradiated ferrihydrite displayed a mixture of poorly crystalline iron phases with the emergence of reflections attributable to 6-line ferrihydrite^{28,30,31} and akaganeite (Figure 1d).³² However, the morphology of the crystallites did not appear different from the nonirradiated sample, and there was no distinct increase in the lattice interference pattern (from alternating high and low electron density) that might be expected with an increase in crystallinity toward 6-line ferrihydrite.²⁶ In addition, irradiated ferrihydrite did show a much lower degree of aggregation (Figure 1c).

Yakabukie et al.³³ found that the structure of γ -FeOOH did not change with prolonged irradiation (134 kGy), although an increase in particle size as a function of irradiation time was reported. In our study, crystallites of ferrihydrite appeared to show a slight increase in acicularity after irradiation (Figure 1c). Acicularity has previously been attributed to the presence of goethite in a ferrihydrite sample (an artifact of the synthesis procedure); however, SAED patterns of our irradiated ferrihydrite showed no evidence of goethite.²⁶ Thus, our observation may be related to radiation induced increases in the

crystallite size rather than a structural alteration, however, the reason for this is unclear.

The Mössbauer spectrum of nonirradiated ferrihydrite was fitted with two Lorentzian doublets, as would be expected for 2-line ferrihydrite (Figure 2).³⁴ The fitting gave an isomer shift of

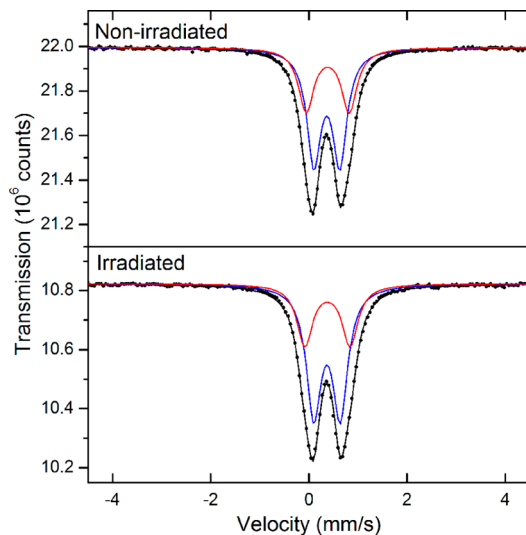


Figure 2. Mössbauer spectra of nonirradiated (top) and irradiated (bottom) ferrihydrite showing calculated fits (black curve) and component fits (red and blue curves). Respective $\chi^2 = 1.27$ and 1.51 .

0.37 mm s^{-1} and quadrupole splitting of 0.53 mm s^{-1} for the first component (comprising $62.2 \pm 4.2\%$ of the fit) and an isomer shift of 0.38 mm s^{-1} and a quadrupole splitting of 0.88 mm s^{-1} for the second component ($37.8 \pm 4.3\%$ of the fit). These values are in good agreement with previously reported Mössbauer parameters for poorly crystalline (2-line) ferrihydrite.^{34,35}

The Mössbauer spectrum obtained after irradiation of this material was best fitted with two Lorentzian doublets (Figure 2), with an isomer shift of 0.37 mm s^{-1} and quadrupole splitting of 0.54 mm s^{-1} for the first doublet (comprising $66.4 \pm 3.9\%$ of the fit) and an isomer shift of 0.38 mm s^{-1} and

quadrupole splitting of 0.93 mm s^{-1} for the second component ($33.6 \pm 4.0\%$ of the fit).

While the relative areas of each doublet in the irradiated material were not significantly different to those of the starting material, nonirradiated ferrihydrite showed a degree of asymmetry in the recorded Mössbauer spectrum (Figure 2). Vandenberghe et al. state that this asymmetry is typical of structural disorder—a defining characteristic of an amorphous material.³⁵ Hence, an increase in symmetry would suggest increased structural ordering post irradiation (Figure 2). Interestingly, the parameters reported for irradiated ferrihydrite are closer to those reported previously for RT measurements on akaganeite than for either 2-line or 6-line ferrihydrite (Table 1),¹⁴ though the authors add the caveat that both ferrihydrite and akaganeite are characterized by similar doublets in their Mössbauer spectra.^{35,36} However, the SAED pattern of irradiated ferrihydrite does display a reflection at 5.71 \AA that may be attributable to the more crystalline akaganeite (Figure 1d).³² Transformation to akaganeite would require chloride to be present in solution. Indeed, ferrihydrite was prepared by hydrolysis of a FeCl_3 solution, and while the precipitate was washed six times via centrifugation and confirmed as 2-line ferrihydrite by XRD, trace amounts of chloride may have been present in solution and therefore partial transformation to akaganeite cannot be ruled out.

The nonirradiated hematite had a morphology consistent with that previously reported for hematite (Figure 3a),²⁷ and the associated SAED pattern contained reflections attributable to the interplanar spacings reported previously (Figure 3b).³⁷ Similarly, the Mössbauer spectrum was constrained by the fitting of two sextets with parameters typical of hematite (Figure 4 and Table 1).¹⁴ While the Mössbauer spectrum of hematite may be expected to contain only one sextet (as hematite contains only one Fe(III) lattice site), previous studies have constrained hematite spectra better with two sextets.^{38,39} These studies base their observations on a study by Shinjo et al. that observed the surface magnetic hyperfine field to be smaller than in the bulk.⁴⁰ Jacob and Abdul Khadar suggest that this difference in site environments of surface and core Fe in nanoparticulate hematite gives rise to the two spectral components.³⁸

Table 1. Mössbauer Parameters of All Samples in This Study and Those Previously Reported for Akaganeite. δ , Isomer Shift; ΔE_Q , Quadrupole Splitting and B_{hf} , Magnetic Hyperfine Field

| sample | Lorentzian component | $\delta \text{ mm s}^{-1}$ | $\Delta E_Q \text{ mm s}^{-1}$ | $B_{hf} \text{ T}$ | RA ^a % |
|--------------------------|----------------------|----------------------------|--------------------------------|--------------------|-------------------|
| ferrihydrite | doublet 1 | $0.37 \pm <0.01$ | $0.53 \pm <0.01$ | | 62 |
| | doublet 2 | $0.38 \pm <0.01$ | 0.88 ± 0.02 | | 38 |
| irradiated ferrihydrite | doublet 1 | $0.37 \pm <0.01$ | $0.54 \pm <0.01$ | | 66 |
| | doublet 2 | $0.38 \pm <0.01$ | 0.93 ± 0.02 | | 34 |
| akaganeite ¹⁴ | 1st component | 0.38 | 0.55 | | |
| | 2nd component | 0.37 | 0.95 | | |
| hematite | doublet 1 | 0.22^b | 0.36^b | | 2 |
| | sextet 1 | $0.39 \pm <0.01$ | $-0.11 \pm <0.01$ | $50.88 \pm <0.01$ | 65 |
| | sextet 2 | $0.37 \pm <0.01$ | $-0.12 \pm <0.01$ | 49.24 ± 0.01 | 33 |
| irradiated hematite | doublet 1 | 0.21 ± 0.01 | 0.27 ± 0.01 | | 45 |
| | sextet 1 | 0.39 ± 0.02 | -0.20^b | 50.4 ± 0.1 | 55 |

^aRA, relative area of signal. ^bValue fixed during fitting to improve fit or because “floating” led to unrealistic parameters.

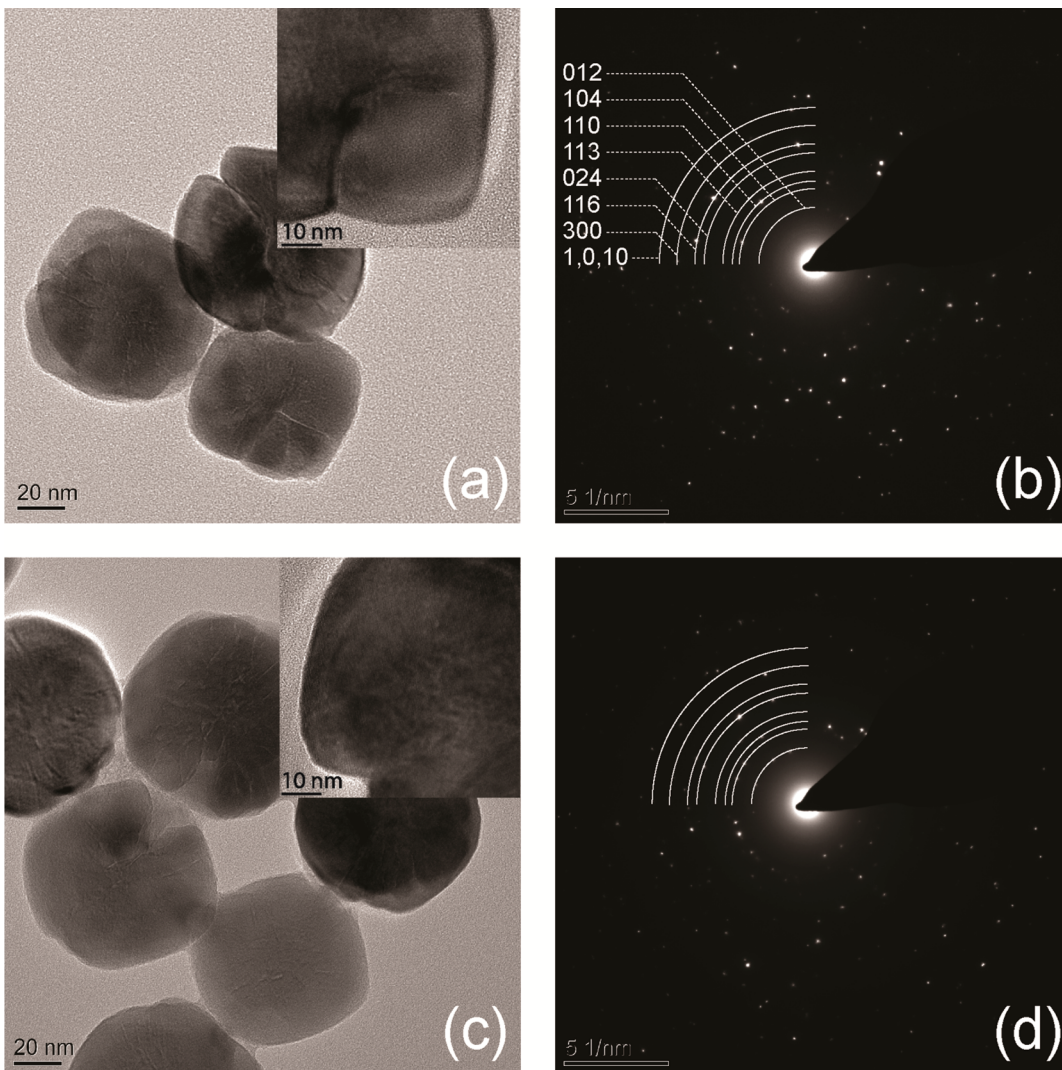


Figure 3. Transmission electron micrographs of nonirradiated (a) and irradiated (c) hematite. Corresponding SAED patterns show indexed lines for hematite in (b) and (d), respectively.

Unlike irradiated ferrihydrite, the SAED pattern for irradiated hematite remains similar to the starting material (Figure 3d). Furthermore, no lattice defects were apparent in TEM images (Figure 3c) and lattice interference patterns were well intersected by crystal edges, that is, no amorphization was apparent at these fringes and no surface depositions of amorphous oxides were visible that could have enhanced the bioavailability of Fe(III).¹⁸

Daub et al. observed a mixture of goethite and magnetite upon gamma irradiation of carbon steel, and, although goethite may be considered more bioavailable than hematite, no evidence for these phases were observed in TEM images or SAED patterns.¹¹ Radiation-induced particle size increase in γ -FeOOH reported by Yakabuskie et al. appears to be more important for less crystalline iron phases,³³ as no alteration in hematite particle sizes was noted after irradiation in our study (nonirradiated hematite mean particle size = 78.09 nm ($n = 132$); irradiated hematite mean particle size = 78.01 nm ($n = 119$)).

Despite the apparent lack of evidence for radiation damage or alteration to hematite in photomicrographs or diffraction patterns, the Mössbauer spectrum of irradiated hematite showed the emergence of a very distinct, paramagnetic Fe(III)

component (room temperature doublet) with a very low isomer shift (0.21 mm s^{-1}) and quadrupole splitting (0.27 mm s^{-1}) comprising 45% of the peak areas (Figure 4 and Table 1). While it is difficult to define this paramagnetic phase, the emergence of this doublet is associated with enhanced Fe(III)-reduction in irradiated hematite systems (discussed below). Thus, given the constraints on microbial reduction of iron oxides,¹⁸ it is suggested that this new phase is a poorly crystalline iron oxide.

Microbial Reduction of Irradiated Oxides. Ferrozine assay results indicated that, as expected, nonirradiated ferrihydrite was readily reduced by *S. oneidensis* as evidenced by an increase to $\sim 50\%$ Fe(II) after 30 days incubation (Figure 5). Despite an increase in crystallinity as observed in SAED patterns and Mössbauer spectra, irradiated ferrihydrite underwent significantly higher levels of iron reduction ($\sim 80\%$). This result is somewhat surprising, as crystallinity has been shown to be a major limiting factor in dissimilatory iron reduction by bacteria, with crystalline phases generally expected to be more recalcitrant to microbial reduction.¹⁸

This observation may be related to the conversion of 2-line ferrihydrite to a phase similar to akaganeite during irradiation, as observed via Mössbauer parameters and SAED patterns. A

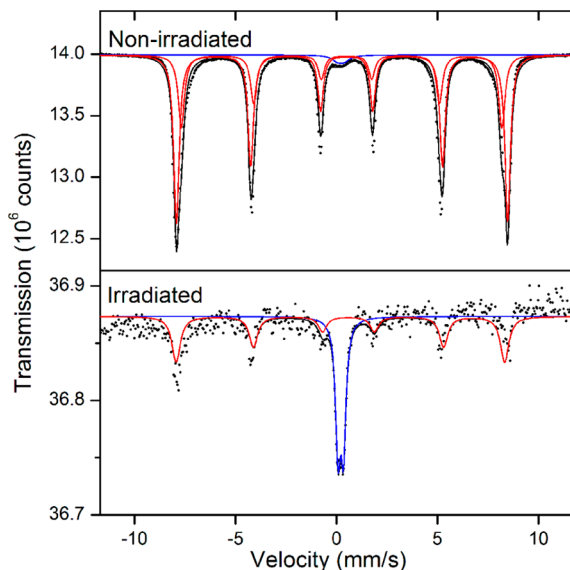


Figure 4. Mössbauer spectra of nonirradiated (top) and irradiated (bottom) hematite showing calculated fits (black curve) and component fits (red and blue curves). Respective reduced $\chi^2 = 214.92$ and 2.45.

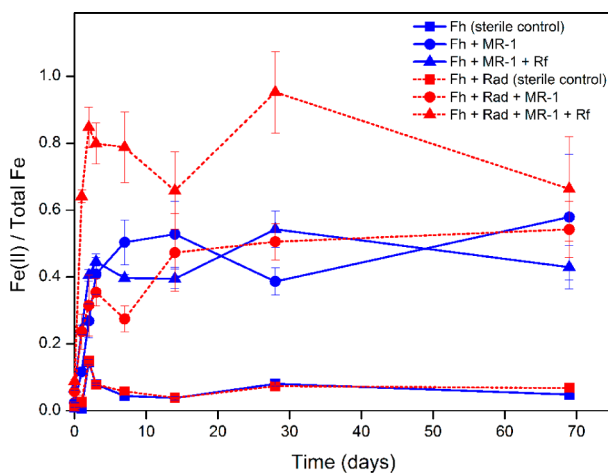


Figure 5. Microbial Fe(III)-reduction in media containing irradiated (red) and nonirradiated (blue) ferrihydrite. Error bars depict the standard error of the mean of triplicate reactors. Fh = ferrihydrite; MR-1 = *S. oneidensis* MR-1; Rf = 10 μM riboflavin.

study by Cutting et al. showed akaganeite is reduced at double the rate of poorly crystalline ferrihydrite, but only in the presence of an electron shuttle.¹⁸ Indeed, we also observed that a doubling in the rate of microbial reduction of irradiated ferrihydrite only occurred with the addition of riboflavin (Figure 5), which acts as an electron shuttling compound.⁴¹

In addition, Cutting et al. suggest that aggregation imparts a large control on iron reduction via a subsequent decrease in effective surface area and, thus, surface site availability.¹⁸ Hence, a decrease in ferrihydrite particle aggregation as a result of irradiation may also explain the high levels of Fe(III) reduction observed.

Figure 6 indicates that nonirradiated hematite is largely recalcitrant to reduction by *S. oneidensis* as expected,¹⁸ though limited levels of iron reduction were observed. However, a similar phenomenon occurred as with irradiated ferrihydrite, with irradiation of hematite yielding a 3-fold increase in

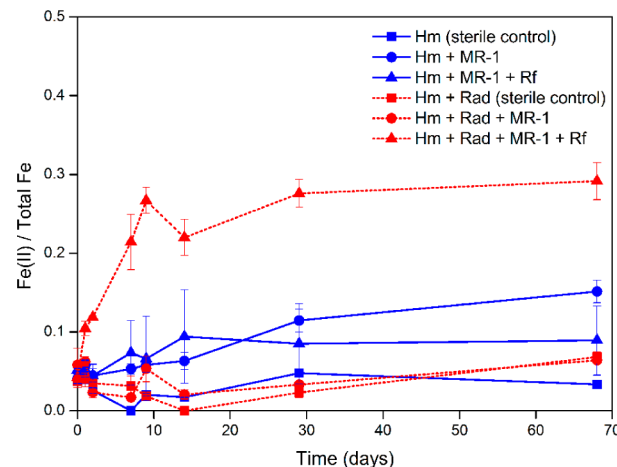


Figure 6. Microbial Fe(III)-reduction in media containing irradiated (red) and nonirradiated (blue) hematite. Error bars depict the standard error of the mean of triplicate reactors. Hm = hematite; MR-1 = *S. oneidensis* MR-1; Rf = 10 μM riboflavin.

microbiologically reduced iron to approximately 30% (Figure 6). Both the rate and extent of production of Fe(II) was increased dramatically with the addition of an electron shuttle, suggesting that any radiation induced changes to the mineral are not directly accessible for enzymatic reduction in this experimental system. Nevertheless, this observation does not preclude the possibility of subtle changes in surface-accessible sites not revealed by TEM. It should be noted that there was some variation between the final extent of Fe(III) reduction across the other treatments, but in all cases, final levels of reduction were far lower in the absence of an electron shuttle and radiation treatment and the rate of reduction was less than 10% of the value noted for irradiated hematite with added riboflavin.

Characterization of Bioreduced Solids. The fate of microbially reduced iron in treatments that exhibited enhanced Fe(II) production as a result of irradiation was probed using powder XRD and Mössbauer spectroscopy. Analysis of the XRD diffractogram of bioreduced solids from experiments containing *S. oneidensis*, the electron shuttle riboflavin and nonirradiated ferrihydrite indicated that bioreduction led to the incorporation of Fe^{2+} in magnetite and siderite (SI Figure S1). Quantitative refinement of the fit suggests that magnetite was the dominant product (approximately $82 \pm 2\%$), with siderite comprising the remaining $\sim 18 \pm 2\%$. Magnetite is typically observed as a biomineralization product of poorly crystalline iron oxide reduction and siderite may also be expected, particularly as the observed $\text{Fe}(\text{II})/\text{(III)}$ ratio is higher than stoichiometric magnetite, likely leading to the additional precipitation of Fe^{2+} with CO_3^{2-} from the bicarbonate buffer used in these experiments.^{24,42,43}

In systems containing irradiated ferrihydrite, XRD and quantitative refinement of the fits suggested that the enhanced Fe(III) reduction led to the incorporation of Fe^{2+} into magnetite (approximately $45 \pm 3\%$), siderite ($\sim 23 \pm 2\%$) and ferrous hydroxy carbonate ($\text{Fe}_2(\text{OH})_2\text{CO}_3$) ($\sim 23 \pm 2\%$) (ICDD PDF 33–0650)⁴⁴ (SI Figure S1). The formation of iron carbonates, e.g. siderite, during bioreduction of poorly crystalline Fe(III) oxides has been linked previously to the total concentration and supply rate of Fe(II), with faster rates leading to enhanced incorporation of Fe^{2+} into carbonate phases.⁴⁵ In addition, ferrous hydroxy carbonate has been observed previously as a stable transformation product of

biogenic magnetite, resulting from the bioreduction of a mixed ferrihydrite and akaganeite substrate by *S. putrefaciens*.⁴⁶ These observations are, therefore, consistent with the irradiation induced transformation of ferrihydrite to akaganeite and subsequent increased rates and extent of bioreduction, followed by enhanced incorporation of Fe²⁺ into siderite and ferrous hydroxy carbonate.

In addition to Fe(II)-bearing phases, a small peak attributable to goethite is also present in the diffractogram of the bioreduced solids originating from irradiated ferrihydrite. Fe²⁺ is known to catalyze the transformation of ferrihydrite to more crystalline oxides, such as goethite, and its appearance may be a result of this.⁴⁵ However, this is a minor component of the sample (approximately 9 ± 2%) and, as such, goethite does not likely represent a dominant end product of bioreduction of irradiated ferrihydrite.

Analysis of the XRD diffractogram of end-product solids from experiments containing *S. oneidensis*, riboflavin and nonirradiated hematite indicated that hematite remained the predominant phase after incubation with *S. oneidensis* (SI Figure S2). Quantitative refinement of the fit indicated that hematite comprised approximately 92 ± <1% of the solids, while the remaining ~8 ± <1% of the solids was identified as siderite. These results are consistent with the analysis of Fe(II) concentrations by Ferrozine assay, which suggested that nonirradiated hematite is largely recalcitrant to reduction by *S. oneidensis*, though limited levels of Fe(II) were produced and incorporated into siderite. In systems containing irradiated hematite, XRD analyses indicated that the enhanced Fe(III) reduction led to significant incorporation of biogenic Fe(II) into siderite (approximately 67 ± <1%), with the remaining ~33 ± <1% of solids identified as hematite. Based on this quantification, the stoichiometry and speciation of Fe in these two phases indicate that ~50% of the total Fe is Fe(II). This is somewhat higher than the ~30% Fe(II) indicated by Ferrozine assay and this discrepancy may be due to the incomplete extraction of Fe(II) from the solids during the 0.5 N HCl extraction for this colorimetric assay.

In addition, the room temperature Mössbauer spectrum of the bioreduced sample containing irradiated hematite exhibits a ferrous doublet with parameters similar to those previously reported for siderite (SI Figure S3; isomer shift of 1.26 ± <0.01 mm s⁻¹ and quadrupole splitting of 1.87 ± <0.01 mm s⁻¹).^{47–50} The relative area of this siderite component was 50.6 ± 0.6% and is in good agreement with the XRD data, predicting ~50% of the total iron to be Fe(II). The remaining features of the Mössbauer spectrum can be constrained by a sextet (relative area of 35.0 ± 1.2%) with very similar parameters to the hematite starting material (isomer shift of 0.39 ± <0.01 mm s⁻¹; a quadrupole splitting of -0.11 ± <0.01 mm s⁻¹ and magnetic hyperfine splitting of 50.38 ± 0.04 T) and a ferric doublet (isomer shift of 0.22 ± 0.02 mm s⁻¹; quadrupole splitting of 0.31 ± 0.08 mm s⁻¹). The parameters of this second doublet are similar to those reported for the paramagnetic ferric phase observed in the irradiated hematite sample prior to incubation with *S. oneidensis* (isomer shift of 0.21 ± 0.01 mm s⁻¹ and quadrupole splitting of 0.27 ± 0.01 mm s⁻¹), though the relative area of this component was significantly decreased after incubation (~45% before and ~14% after incubation). Thus, these data are consistent with our hypothesis that irradiation led to the formation of an amorphous Fe(III) phase that was readily reduced during incubation with *S. oneidensis*.

The incorporation of Fe²⁺ into siderite is not surprising given the use of a bicarbonate buffer in these experiments.

Although future work is clearly warranted to gain a deeper insight into the mineralogical changes that underpin the phenomena reported in this study (including further work on the phases formed and the impact of particle aggregation in a range of experimental systems), it is clear our results show that Fe(III) minerals are susceptible to radiation alteration which can alter their bioavailability for microbial reduction. At present, safety cases for radwaste geological disposal facilities lack information on key microbial processes. Iron-based materials will be prevalent in the waste-forms, containers and structures in many repository designs, that is, for intermediate level waste in the UK,⁵¹ and after a period of corrosion, have the potential to influence biogeochemical evolution of the facility. The microbial reduction of Fe(III) may be enhanced by radiation alteration and could be promoted further by the production of electron donors such as hydrogen and organic compounds formed by the radiolysis of water and polymers, respectively.^{51–55} Stimulation of dissimilatory Fe(III)-reduction may promote direct enzymatic or indirect (e.g., via biogenic Fe(II)) reduction of important redox-sensitive radionuclides, such as U(VI) and Tc(VII), and could, therefore, play an important role in controlling radionuclide migration.^{1–6} Thus, enhanced radiation inputs could provide the basis of a novel ecosystem capable of exerting important influences on the biogeochemical evolution of a radwaste geological disposal facility.

ASSOCIATED CONTENT

Supporting Information

Additional information as noted in the text. This material is available free of charge via the Internet at <http://pubs.acs.org/>.

AUTHOR INFORMATION

Corresponding Author

*E-mail: ashley.r.brown@manchester.ac.uk.

Notes

The authors declare no competing financial interest.

[†]Author deceased.

ACKNOWLEDGMENTS

This work was funded by a BBSRC studentship awarded to A.R.B. (Grant BB/F017472/1) and CASE funding from the Nuclear Decommissioning Authority. The DCF is a joint initiative of the Nuclear Decommissioning Authority and The University of Manchester. The research of J. A. LaVerne as described herein was supported through the Division of Chemical Sciences, Geosciences and Biosciences, Basic Energy Sciences, Office of Science, United States Department of Energy through grant number DE-FC02-04ER15533. This is contribution number NDRL 4995 from the Notre Dame Radiation Laboratory. We gratefully acknowledge Calum Patrick for assisting with UV/vis measurements, John Waters for powder XRD data acquisition and Michael Ward at the Leeds EPSRC Nanoscience and Nanotechnology Facility (supported by Grant EP/K023853/1) for carrying out TEM and SAED. We thank Michelle Scherer, University of Iowa, and James Byrne, University of Tübingen, for helpful comments during preparation of the manuscript. We also note the sad loss of Paul Wincott who contributed significantly to this work.

■ REFERENCES

- (1) Lloyd, J. R.; Macaskie, L. E. A novel PhosphorImager-based technique for monitoring the microbial reduction of technetium. *Appl. Environ. Microbiol.* **1996**, *62*, 578–582.
- (2) Lloyd, J. R.; Sole, V. A.; Van Praagh, C. V. G.; Lovley, D. R. Direct and Fe(II)-mediated reduction of technetium by Fe(III)-reducing bacteria. *Appl. Environ. Microbiol.* **2000**, *66*, 3743–3749.
- (3) Hansel, C. M.; Wielinga, B. W.; Fendorf, S. R. Structural and compositional evolution of Cr/Fe solids after indirect chromate reduction by dissimilatory iron-reducing bacteria. *Geochim. Cosmochim. Acta* **2003**, *67*, 401–412.
- (4) Wilkins, M. J.; Livens, F. R.; Vaughan, D. J.; Lloyd, J. R. The impact of Fe(III)-reducing bacteria on uranium mobility. *Biogeochemistry* **2006**, *78*, 125–150.
- (5) Wildung, R. E.; Gorby, Y. A.; Krupka, K. M.; Hess, N. J.; Li, S. W.; Plymale, A. E.; McKinley, J. P.; Fredrickson, J. K. Effect of electron donor and solution chemistry on products of dissimilatory reduction of technetium by *Shewanella putrefaciens*. *Appl. Environ. Microbiol.* **2000**, *66*, 2451–2460.
- (6) Williams, K. H.; Long, P. E.; Davis, J. A.; Wilkins, M. J.; N'Guessan, A. L.; Steefel, C. I.; Yang, L.; Newcomer, D.; Spane, F. A.; Kerkhof, L. J.; McGuinness, L.; Dayvault, R.; Lovley, D. R. Acetate availability and its influence on sustainable bioremediation of uranium-contaminated groundwater. *Geomicrobiol. J.* **2011**, *28*, 519–539.
- (7) Fredrickson, J. K.; Zachara, J. M.; Balkwill, D. L.; Kennedy, D.; Li, S. M. W.; Kostandarithes, H. M.; Daly, M. J.; Romine, M. F.; Brockman, F. J. Geomicrobiology of high-level nuclear waste-contaminated vadose sediments at the Hanford Site, Washington State. *Appl. Environ. Microbiol.* **2004**, *70*, 4230–4241.
- (8) Lloyd, J. R. Microbial reduction of metals and radionuclides. *FEMS Microbiol. Rev.* **2003**, *27*, 411–425.
- (9) NDA. *Geological Disposal: Near-Field Evolution Status Report*, NDA/RWMD/033; Nuclear Decommissioning Authority, 2010.
- (10) Allard, T.; Calas, G. Radiation effects on clay mineral properties. *Appl. Clay Sci.* **2009**, *43*, 143–149.
- (11) Daub, K.; Zhang, X.; Noel, J. J.; Wren, J. C. Gamma-radiation-induced corrosion of carbon steel in neutral and mildly basic water at 150 degrees C. *Corros. Sci.* **2011**, *53*, 11–16.
- (12) Zhang, X.; Xu, W.; Shoesmith, D. W.; Wren, J. C. Kinetics of H₂O₂ reaction with oxide films on carbon steel. *Corros. Sci.* **2007**, *49*, 4553–4567.
- (13) Ladrière, J. Irradiation effects detected by Mössbauer spectroscopy in iron complexes. *Hyperfine Interact.* **1998**, *113*, 411–418.
- (14) Cornell, R. M.; Schwertmann, U. *The Iron Oxides*; VCH: New York, 2003.
- (15) Roden, E. E. Fe(III) oxide reactivity toward biological versus chemical reduction. *Environ. Sci. Technol.* **2003**, *37*, 1319–1324.
- (16) Roden, E. E. Geochemical and microbiological controls on dissimilatory iron reduction. *C. R. Geosci.* **2006**, *338*, 456–467.
- (17) Hansel, C. M.; Benner, S. G.; Nico, P.; Fendorf, S. Structural constraints of ferric (hydr)oxides on dissimilatory iron reduction and the fate of Fe(II). *Geochim. Cosmochim. Acta* **2004**, *68*, 3217–3229.
- (18) Cutting, R. S.; Coker, V. S.; Fellowes, J. W.; Lloyd, J. R.; Vaughan, D. J. Mineralogical and morphological constraints on the reduction of Fe(III) minerals by *Geobacter sulfurreducens*. *Geochim. Cosmochim. Acta* **2009**, *73*, 4004–4022.
- (19) Reed, D. T.; Scott, D. D.; Weiner, M. F. Gamma and alpha radiation levels in a basalt high-level waste repository: potential impact on container corrosion and packing properties. In *Coupled Processes Associated with Nuclear Waste Repositories*; Tsang, C.-F., Ed.; Academic Press: Orlando, 1987; pp 325 – 338.
- (20) Plotze, M.; Kahr, G.; Stengele, R. H. Alteration of clay minerals - gamma-irradiation effects on physicochemical properties. *Appl. Clay Sci.* **2003**, *23*, 195–202.
- (21) Allard, T.; Balan, E.; Calas, G.; Fourdrin, C.; Morichon, E.; Sorieul, S. Radiation-induced defects in clay minerals: A review. 2012, *277*, 112–120.
- (22) Downs, R. T.; Hall-Wallace, M. The American mineralogist crystal structure database. *Am. Mineral.* **2003**, *88*, 247–250.
- (23) Myers, C. R.; Nealson, K. H. Bacterial manganese reduction and growth with manganese oxide as the sole electron-acceptor. *Science* **1988**, *240*, 1319–1321.
- (24) Lovley, D. R.; Phillips, E. J. P. Availability of ferric iron for microbial reduction in bottom sediments of the fresh-water tidal Potomac river. *Appl. Environ. Microbiol.* **1986**, *52*, 751–757.
- (25) Lovley, D. R.; Phillips, E. J. P. Organic-matter mineralization with reduction of ferric iron in anaerobic sediments. *Appl. Environ. Microbiol.* **1986**, *51*, 683–689.
- (26) Janney, D. E.; Cowley, J. M.; Buseck, P. R. Transmission electron microscopy of synthetic 2-and 6-line ferrihydrite. *Clays Clay Miner.* **2000**, *48*, 111–119.
- (27) Schwertmann, U.; Cornell, R. M. *Iron Oxides in the Laboratory*; Weinheim: New York, 1991.
- (28) Manceau, A.; Druts, V. A. Local-structure of ferrihydrite and feroxyhite by EXAFS spectroscopy. *Clay Miner.* **1993**, *28*, 165–184.
- (29) Janney, D. E.; Cowley, J. M.; Buseck, P. R. Structure of synthetic 2-line ferrihydrite by electron nanodiffraction. *Am. Mineral.* **2000**, *85*, 1180–1187.
- (30) Jansen, E.; Kyek, A.; Schafer, W.; Schwertmann, U. The structure of six-line ferrihydrite. *Appl. Phys. A: Mater. Sci. Process.* **2002**, *74*, S1004–S1006.
- (31) Michel, F. M.; Ehm, L.; Antao, S. M.; Lee, P. L.; Chupas, P. J.; Liu, G.; Strongin, D. R.; Schoonen, M. A. A.; Phillips, B. L.; Parise, J. B. The structure of ferrihydrite, a nanocrystalline material. *Science* **2007**, *316*, 1726–1729.
- (32) Post, J. *Akaganeite ICDD file no. 00–042–1315*; National Museum of Natural History; Smithsonian Institution: Washington D.C., 1989.
- (33) Yakabuskie, P. A.; Joseph, J. M.; Keech, P.; Botton, G. A.; Guzonas, D.; Wren, J. C. Iron oxyhydroxide colloid formation by gamma-radiolysis. *Phys. Chem. Chem. Phys.* **2011**, *13*, 7167–7175.
- (34) Murad, E.; Schwertmann, U. The Mössbauer spectrum of ferrihydrite and its relations to those of other iron oxides. *Am. Mineral.* **1980**, *65*, 1044–1049.
- (35) Vandenberghe, R. E.; Degrave, E.; Landuydt, C.; Bowen, L. H. Some aspects concerning the characterization of iron oxides and hydroxides in soils and clays. *Hyperfine Interact.* **1990**, *53*, 175–195.
- (36) Childs, C. W.; Johnston, J. H. Mössbauer-spectra of proto-ferrihydrite at 77 and 295 K, and a reappraisal of the possible presence of akaganeite in New Zealand soils. *Aust. J. Soil Res.* **1980**, *18*, 245–250.
- (37) Blake, R. L.; Hessevic, R.; Zoltai, T.; Finger, L. W. Refinement of the hematite structure. *Am. Mineral.* **1966**, *51*, 123–129.
- (38) Jacob, J.; Abdul Khadar, M. VSM and Mössbauer study of nanostructured hematite. *J. Magn. Magn. Mater.* **2010**, *322*, 614–621.
- (39) Musić, S.; Czakó-Nagy, I.; Salaj-Obelić, I.; Ljubešić, N. Formation of α -Fe₂O₃ particles in aqueous medium and their properties. *Mater. Lett.* **1997**, *32*, 301–305.
- (40) Shinjo, T.; Kiyama, M.; Sugita, N.; Watanabe, K.; Takada, T. Surface magnetism of α -Fe₂O₃ by Mössbauer spectroscopy. *J. Magn. Magn. Mater.* **1983**, *35*, 133–135.
- (41) von Canstein, H.; Ogawa, J.; Shimizu, S.; Lloyd, J. R. Secretion of flavins by *Shewanella* species and their role in extracellular electron transfer. *Appl. Environ. Microbiol.* **2008**, *74*, 615–623.
- (42) Perez-Gonzalez, T.; Jimenez-Lopez, C.; Neal, A. L.; Rull-Perez, F.; Rodriguez-Navarro, A.; Fernandez-Vivas, A.; Iñez-Pareja, E. Magnetite biominerization induced by *Shewanella oneidensis*. *Geochim. Cosmochim. Acta* **2010**, *74*, 967–979.
- (43) Fredrickson, J. K.; Zachara, J. M.; Kennedy, D. W.; Dong, H.; Onstott, T. C.; Hinman, N. W.; Li, S.-m. Biogenic iron mineralization accompanying the dissimilatory reduction of hydrous ferric oxide by a groundwater bacterium. *Geochim. Cosmochim. Acta* **1998**, *62*, 3239–3257.
- (44) Erdös, E.; Altorfer, H. Ein dem Malachit ähnliches basisches Eisenkarbonat als Korrosionsprodukt von Stahl. *Mater. Corros.* **1976**, *27*, 304–312.
- (45) Zachara, J. M.; Kukkadapu, R. K.; Fredrickson, J. K.; Gorby, Y. A.; Smith, S. C. Biominerization of poorly crystalline Fe(III) oxides

by dissimilatory metal reducing bacteria (DMRB). *Geomicrobiol. J.* **2002**, *19*, 179–207.

(46) Kukkadapu, R. K.; Zachara, J. M.; Fredrickson, J. K.; Kennedy, D. W.; Dohnalkova, A. C.; McCready, D. E. Ferrous hydroxy carbonate is a stable transformation product of biogenic magnetite. *Am. Mineral.* **2005**, *90*, 510–515.

(47) Readman, P. W.; Coey, J. M. D.; Mosser, C.; Weber, F. Analysis of some lake sediments from Greece. *J. Phys., Colloq.* **1976**, *37*, 845–848.

(48) Musić, S.; Popović, S. Mössbauer spectroscopic and X-ray diffraction study of the thermal decomposition of natural siderite and goethite. *J. Radioanal. Nucl. Chem.* **1987**, *111*, 27–41.

(49) Wade, M. L.; Agresti, D. G.; Wdowiak, T. J.; Armendarez, L. P.; Farmer, J. D. A Mössbauer investigation of iron-rich terrestrial hydrothermal vent systems: Lessons for Mars exploration. *J. Geophys. Res.: Planets* **1999**, *104*, 8489–8507.

(50) Chistyakova, N. I.; Rusakov, V. S.; Shapkin, A. A.; Zhilina, T. N.; Zavarzina, D. G. Reduction of amorphous Fe(III)-hydroxide by binary microbial culture, a Mössbauer study. *Hyperfine Interact.* **2010**, *197*, 325–330.

(51) Lin, L.-H.; Slater, G. F.; Sherwood Lollar, B.; Lacrampe-Couloume, G.; Onstott, T. C. The yield and isotopic composition of radiolytic H₂, a potential energy source for the deep subsurface biosphere. *Geochim. Cosmochim. Acta* **2005**, *69*, 893–903.

(52) Lin, L. H.; Wang, P. L.; Rumble, D.; Lippmann-Pipke, J.; Boice, E.; Pratt, L. M.; Lollar, B. S.; Brodie, E. L.; Hazen, T. C.; Andersen, G. L.; DeSantis, T. Z.; Moser, D. P.; Kershaw, D.; Onstott, T. C. Long-term sustainability of a high-energy, low-diversity crustal biome. *Science* **2006**, *314*, 479–482.

(53) Galès, G.; Libert, M.-F.; Sellier, R.; Cournac, L.; Chapon, V.; Heulin, T. Molecular hydrogen from water radiolysis as an energy source for bacterial growth in a basin containing irradiating waste. *FEMS Microbiol. Lett.* **2004**, *240*, 155–162.

(54) Libert, M.; Bildstein, O.; Esnault, L.; Jullien, M.; Sellier, R. Molecular hydrogen: An abundant energy source for bacterial activity in nuclear waste repositories. *Phys. Chem. Earth* **2011**, *36*, 1616–1623.

(55) Askarieh, M. M.; Chambers, A. V.; Daniel, F. B. D.; FitzGerald, P. L.; Holtom, G. J.; Pilkington, N. J.; Rees, J. H. The chemical and microbial degradation of cellulose in the near field of a repository for radioactive wastes. *Waste Manage.* **2000**, *20*, 93–106.